astro-ph/0601111

September 2006

Explosive Nucleosynthesis in GRB Jets Accompanied by Hypernovae

Shigehiro Nagataki[1,2], Akira Mizuta[3], Katsuhiko Sato[4,5]

ABSTRACT

Two-dimensional hydrodynamic simulations are performed to investigate explosive nucleosynthesis in a collapsar using the model of MacFadyen and Woosley (1999). It is shown that ^{56}Ni is not produced in the jet of the collapsar sufficiently to explain the observed amount of a hypernova when the duration of the explosion is $\sim$10 sec, which is considered to be the typical timescale of explosion in the collapsar model. Even though a considerable amount of ^{56}Ni is synthesized if all explosion energy is deposited initially, the opening angles of the jets become too wide to realize highly relativistic outflows and gamma-ray bursts in such a case. From these results, it is concluded that the origin of ^{56}Ni in hypernovae associated with GRBs is not the explosive nucleosynthesis in the jet. We consider that the idea that the origin is the explosive nucleosynthesis in the accretion disk is more promising. We also show that the explosion becomes bi-polar naturally due to the effect of the deformed progenitor. This fact suggests that the ^{56}Ni synthesized in the accretion disk and conveyed as outflows are blown along to the rotation axis, which will explain the line features of SN 1998bw and double peaked line features of SN 2003jd. Some fraction of the gamma-ray lines from ^{56}Ni decays in the jet will appear without losing their energies because the jet becomes optically thin before a considerable amount of ^{56}Ni decays as long as the jet is a relativistic flow, which may be observed as relativistically Lorentz boosted line profiles in future. We show that abundance of nuclei whose mass

[1]Yukawa Institute for Theoretical Physics, Kyoto University, Oiwake-cho Kitashirakawa Sakyo-ku, Kyoto 606-8502, Japan, E-mail: nagataki@yukawa.kyoto-u.ac.jp

[2]KIPAC, Stanford University, P.O.Box 20450, MS 29, Stanford, CA, 94309, USA

[3]Max-Planck-Institute für Astrophysik, Karl-Schwarzschild-Str. 1, 85741 Garching, Germany

[4]Department of Physics, The University of Tokyo, Bunkyo-ku, Tokyo 113-0033, Japan

[5]Research Center for the Early Universe (RESCEU), The University of Tokyo, Tokyo 113-0033, Japan

Submitted to Astrophys.J.

Work supported in part by Department of Energy contract DE-AC02-76SF00515

number $\sim$ 40 in the ejecta depends sensitively on the energy deposition rate, which is a result of incomplete silicon burning and alpha-rich freezeout. So it may be determined by observations of chemical composition in metal poor stars which model is the proper one as a model of a gamma-ray burst accompanied by a hypernova.

Subject headings: gamma rays: bursts — accretion, accretion disks — black hole physics — nuclear reactions, nucleosynthesis, abundances — supernovae: general — galaxy: halo

1. INTRODUCTION

There has been growing evidence linking long gamma-ray bursts (GRBs; in this study, we consider only long GRBs, so we call long GRBs as GRBs hereafter for simplicity) to the death of massive stars. The host galaxies of GRBs are star-forming galaxies and the position of GRBs appear to trace the blue light of young stars (Vreeswijk et al. 2001; Bloom et al. 2002; Gorosabel et al. 2003). Also, 'bumps' observed in some afterglows can be naturally explained as contribution of bright supernovae (Bloom et al. 1999; Reichart 1999; Galama et al. 2000; Garnavich et al. 2003). Moreover, direct evidences of some GRBs accompanied by supernovae have been reported such as the association of GRB 980425 with SN 1998bw (Galama et al. 1998; Iwamoto et al. 1998) and that of GRB 030329 with SN 2003dh (Hjorth et al. 2003; Price et al. 2003; Stanek et al. 2003).

It should be noted that these supernovae are categorized as a new type of supernovae with large kinetic energy ($\sim 10^{52}$ ergs), nickel mass ($\sim 0.5 M_{\odot}$), and luminosity (Iwamoto et al. 1998; Woosley et al. 1999), so these supernovae are sometimes called as hypernovae. Also, since GRBs are considered to be jet-like phenomena (Rhoads 1999; Stanek et al. 1999), it is natural to consider the accompanying supernova to be jet-induced explosion (MacFadyen & Woosley 1999; Khokhlov et al. 1999). It is radioactive nuclei, ^{56}Ni and its daughter nuclei, ^{56}Co, that brighten the supernova remnant and determine its bolometric luminosity. ^{56}Ni is considered to be synthesized through explosive nucleosynthesis because its half-life is very short (5.9 days). So it is natural to consider explosive nucleosynthesis in jet-induced explosion to understand GRBs accompanied by hypernovae.

Nagataki et al. (1997) have done a numerical calculation of explosive nucleosynthesis taking account of effects of jet-induced explosion in the context of normal core-collapse supernova explosion whose explosion energy is set to be 10^{51} erg. They found that ^{56}Ni is much produced in the jet region, which means that much explosive nucleosynthesis occurs

around the jet region. Also, it was found that velocity distribution of iron becomes double peaked due to the asperical explosion and explosive nucleosynthesis (Nagataki et al. 1998a; Nagataki 2000). It was also found that the velocity distribution, which will be observed as a line profile, depends on the angle between our line of sight and rotation axis (Nagataki 2000). Maeda et al. (2002) have done a numerical calculation of explosive nucleosynthesis taking account of effects of jet-induced explosion in the context of hypernovae whose explosion energy is set to be 10^{52} erg. They have shown that sufficient mass of ^{56}Ni enough to explain the observation of hypernovae ($\sim 0.5 M_{\odot}$) can be synthesized around the jet region when the explosion energy is set to be 10^{52} erg. They have also calculated line profiles of [Fe_{II}] blend and of [O_I] from one-dimensional non-LTE nebular code (Mazzali et al. 2001) and found that these line profiles depend on the angle between our line of sight and the direction of the jet. Recently, it was reported that an asymmetric hypernovae, SN 2003jd reveal double-peaked profiles in the nebular lines of neutral oxygen and magnesium (Mazzali et al. 2005).

However, here is one question: whether the difference between explosion energies of 10^{51} erg and 10^{52} is important or not? What does the different explosion energy mean? The answer is 'Yes'. It is impossible to overemphasize its importance because the scenario of explosion has to be dramatically changed to explain the energetic explosion energy of 10^{52} and to realize a GRB.

Nagataki et al. (1997) investigated explosive nucleosynthesis taking account of effects of jet-induced explosion in the context of normal core-collapse supernova explosion, because there is a possibility that normal core-collapse supernova becomes jet-like when effects of rotation are taken into account (Yamada & Sato 1994; Shimizu et al. 1994; Kotake et al. 2003). In this scenario, the typical timescale of core-collapse supernovae is as short as $\sim$ 500 ms (Wilson 1985). So the surrounding layers of iron core does not collapse so much. As a result, the progenitor outside the iron core can not be deformed due to the collapse. This fact supports the treatment of using a spherical progenitor when explosive nucleosynthesis is investigated. Note that the central iron core collapses to a neutron star and it is enough to calculate explosive nucleosynthesis in a spherical outer layer such as Si-, O-, and He-rich layers in the case of normal core-collapse supernovae (Nagataki et al. 1997; Nagataki et al. 1998a; Nagataki et al. 1998b; Nagataki 2000). Also, to initiate the explosion, the explosion energy is deposited around the Si-rich layer as an initial condition in their works. This is justified because the timescale of explosion is very short.

On the other hand, the central engine of GRBs accompanied by hypernovae is not known well. But it is generally considered that normal core-collapse supernovae can not cause an energetic explosion of the order of 10^{52} erg. So another scenario has to be considered to explain the system of GRBs associated with hypernovae. One of the most promising sce-

nario is the collapsar scenario (Woosley 1993). In the collapsar scenario, a black hole is formed as a result of gravitational collapse. Also, rotation of the progenitor plays an essential role. Due to the rotation, an accretion disk is formed around the equatorial plane. On the other hand, the matter around the rotation axis falls into the black hole. It was pointed out that the jet-induced explosion along to the rotation axis occurs due to the heating through neutrino anti-neutrino pair annihilation that are emitted from the accretion disk. MacFadyen and Woosley (1999) demonstrated the numerical simulations of the collapsar, showing that the jet is launched ~ 7 sec after the gravitational collapse and the duration of the jet is about 10 sec, which is comparable to the typical observed duration of GRBs (Mazet et al. 1981; Kouveliotou et al. 1993; Lamb et al. 1993). This timescale is much longer than the typical timescale of normal core-collapse supernovae. As a result, the progenitor becomes deformed even at the Si-rich and O-rich layer in the collapsar model (MacFadyen & Woosley 1999). In particular, the density around the rotation axis becomes low because considerable amount of the matter falls into the black hole, which is a good environment to produce a fire ball (Woltjer 1966; Rees 1967).

Maeda et al. (2002) investigated explosive nucleosynthesis taking account of effects of jet-induced explosion in the context of hypernovae whose energy is 10^{52} erg using the spherical progenitor model and depositing explosion energy at the inner most region initially. However, this treatment seems to be incompatible with the collapsar scenario. The importance of the duration of explosion, ~ 10 sec, is investigated in some papers (Nagataki 2003; Maeda & Nomoto 2003) and it was concluded that the abundance of ^{56}Ni synthesized during explosion depends sensitively on the duration of explosion (i.e. energy deposition rate) and ^{56}Ni is not produced sufficiently to explain the observed amount of $\sim 0.5 M_{\odot}$ when the timescale of explosion becomes as long as 10 sec. In fact, MacFadyen and Woosley (1999) discussed that enough ^{56}Ni should not be synthesized in the jet in the collapsar model. Rather, they pointed out the possibility that a substantial amount of ^{56}Ni is produced in the accretion disk and a part of it is conveyed outwards by the viscosity-driven wind (MacFadyen & Woosley 1999; Pruet et al. 2002). There is another question. Does all of ^{56}Ni produced in the jet of the collapsar model brighten the supernova remnant? If the jet becomes optically thin before ^{56}Ni decays into ^{56}Co and ^{56}Co decays into ^{56}Fe, these nuclei should result in emitting gamma-rays rather than brightening the supernova remnant.

Let us summarize our motivation. We want to understand how collapsars produce a GRB jet and how collapsars eject sufficiently enough ^{56}Ni to explain the luminosity of hypernovae. We want to seek the self-consistent theory of GRB/Hypernova connection. As a first step, we want to consider in this work the consistency between the collapsar model of MacFadyen and Woosley (1999) and explosive nucleosynthesis in a hypernova jet. Can a hypernova jet cause a GRB jet and a sufficiently enough explosive nucleosynthesis to explain

the luminosity of hypernova? Rather, should we consider the GRB jet is different from the hypernova jet? Moreover, should we consider ^{56}Ni comes from the explosive nucleosynthesis in the hypernova jet? Rather, should we consider ^{56}Ni comes from a different site? We want to know the answer. This is our motivation of this work.

Due to the motivation mentioned above. We investigate explosive nucleosynthesis in the context of the collapsar model. We use the collapsar model of MacFadyen and Woosley (1999) in which effects of rotation is included. As a result, the progenitor becomes deformed significantly as mentioned above. We show that ^{56}Ni is not produced sufficiently to explain the observed amount when the duration of the explosion is $\sim$10 sec, which is consistent with the previous works (Nagataki 2003; Maeda & Nomoto 2003). A fine tuning is required to explain the amount of ^{56}Ni by the explosive nucleosynthesis in the jet. This result bring us to the conclusion that the origin of ^{56}Ni in hypernovae associated with GRBs is not the explosive nucleosynthesis in the jet but the one in the accretion disk. We also show that the explosion becomes bi-polar naturally due to the effect of deformed progenitor. This fact suggests that the ^{56}Ni synthesized in the accretion disk and conveyed as outflows are blown along to the rotation axis, which can explain the line features of SN 1998bw and double peaked line features of SN 2003jd (Mazzali et al. 2005). Also we predict that some fraction of gamma-ray lines from ^{56}Ni decays in the jet may show relativistically Lorentz boosted line profiles, which might be observed in future.

2. METHOD OF CALCULATION

We present our method of calculation in this study. We take account of some effects that had not been included in Nagataki et al. (2003). In this study, effects of gravitation and rotation are included. We also adopt realistic equation of state (EOS) of Blinnikov et al. (1996). Furthermore, we adopt an asymmetric progenitor model obtained by MacFadyen and Woosley (1999). So we believe we have done more realistic calculation of explosive nucleosynthesis in this study compared with Nagataki et al. (2003).

We realize the jet-induced explosion by injecting thermal energy around the polar region in the same way as MacFadyen and Woosley (1999) and Aloy et al. (2000). After such a hydrodynamic calculation, we calculate the products of explosive nucleosynthesis as a post-processing. We explain our detailed method of calculation in the following subsections.

2.1. Hydrodynamics

2.1.1. The Scheme

We have done two-dimensional hydrodynamic simulations taking account of self-gravity and gravitational potential of the central point mass. The calculated region corresponds to a quarter of the meridian plane under the assumption of axisymmetry and equatorial symmetry. The spherical mesh with $250(r)\times$ $30(\theta)$ grid points is used for all the computations. The radial grid is nonuniform, extending from 2.0×10^7 cm to 3.0×10^{11} cm with finer grids near the center, while the polar grid is uniform.

The basic equations in the following form are finite differenced on the spherical coordinates:

$$\frac{D\rho}{Dt} = -\rho\nabla\cdot\mathbf{v} \tag{1}$$

$$\rho\frac{D\mathbf{v}}{Dt} = -\nabla p - \rho\nabla\Phi \tag{2}$$

$$\rho\frac{D}{Dt}\left(\frac{e}{\rho}\right) = -p\nabla\cdot\mathbf{v}, \tag{3}$$

where ρ, $\mathbf{v}$, P, Φ, and e are density, velocity, gravitational potential, and internal energy density, respectively. The Lagrangian derivative is denoted as D/Dt. The gravitational potential of the central point mass is modified to account for some of the effects of general relativity (Paczyński & Witta 1980), $\phi = -GM/(r - r_{\rm s})$ where $r_{\rm s} = 2GM/c^2$ is the Schwartzshild radius. The ZEUS-2D code developed by Stone and Norman (1992) has been used with an EOS of an electron-positron gas, which is in thermal equilibrium with blackbody radiation and ideal gas of nuclei (Blinnikov et al. 1996). Since contribution of ideal gas of nuclei to the total pressure is negligible relative to those of electron-positron gas and thermal radiation, we fixed the mean atomic weight in the EOS to be 16 to calculate total pressure and temperature using this EOS.

2.1.2. Initial and Boundary Conditions

We adopt the $9.15M_\odot$ collapsar model of MacFadyen and Woosley (1999). When the central black hole has acquired a mass of 3.762 $M_\odot$, we map the model to our computational grid. The surface of the helium star is $R_* = 2.98\times10^{10}$ cm. Electron fraction, Y_e, is set to be 0.5 throughout of this paper since neutrino process is not included.

To realize the jet-induced explosion, we deposit only thermal energy at a rate $\dot{E} = 10^{51}$ ergs s^{-1} homogeneously within a 30° cone around the rotation axis for 10 sec. In the radial

direction, the deposition region extends from the inner grid boundary located at 200km to a radius of 600 km. This treatment is same as Aloy et al. (2000). We name this model as Model E51. We consider this model as the standard one. For comparison, we perform a calculation in which total explosion energy (= 10^{52} ergs) is put initially with the deposition region same as Model E51. Also, we perform a calculation in which total explosion energy is put initially in a spherically symmetric way (from 200km to 600km). We name these models as Model E52 and E52S, respectively. We consider that these models represent extreme cases. Models in this study are summarized in Table 1.

As for the boundary condition in the radial direction, we adopt the inflow boundary condition for the inner boundary while the outflow boundary condition is used for the outer boundary. That is, the flow toward the central black hole is prohibited at the inner boundary and the inflow from the surface of the progenitor is prohibited at the outer boundary. This is because we consider the phenomenon of explosion, in which the free fall timescale at the inner boundary will be longer than that of explosion. It is also noted that we checked that results of explosive nucleosynthesis do not depend on the inner boundary condition sensitively by changing the inflow boundary condition to the outflow boundary condition for the inner boundary condition. As for the boundary condition in the zenith angle direction, axix of symmetry boundary condition is adopted for the rotation axis, while reflecting boundary condition is adopted for the equatorial plane.

2.2. Explosive Nucleosynthesis

2.2.1. Test Particle Method

Since the hydrodynamics code is Eulerian, we use the test particle method (Nagataki et al. 1997) in order to obtain the informations on the time evolution of the physical quantities along the fluid motion, which are then used for the calculations of the explosive nucleosynthesis. Test particles are scattered in the progenitor and are set at rest initially. They move with the local fluid velocity at their own positions after the passage of the shock wave. The temperature and density that each test particle experiences at each time step are preserved.

Calculations of hydrodynamics and explosive nucleosynthesis are performed separately, since the entropy produced during the explosive nucleosynthesis is much smaller ($\sim$ a few%) than that generated by the shock wave. In calculating the total yields of elements, we assume that each test particle has its own mass determined from their initial distribution so that their sum becomes the mass of the layers where these are scattered. It is also assumed that the nucleosynthesis occurs uniformly in each mass element. These assumptions will be

justified since the movement of the test particles is not chaotic (i.e. the distribution of test particles at the final time still reflects the given initial condition) and the intervals of test particles are sufficiently narrow to give a smooth distribution of the chemical composition in the ejecta. The number of the test particles are 1500. The test particles are put non-uniformly in the radial direction, extending from 2.0×10^7 cm to 3.0×10^{10} cm with closely separated near the center, while they are put uniformly in the polar direction.

2.2.2. Post-Processing

Since the chemical composition behind the shock wave is not in nuclear statistical equilibrium, the explosive nucleosynthesis has to be calculated using the time evolution of (ρ, T) and a nuclear reaction network, which is called post-processing. We use the data of (ρ, T) comoving with the matter obtained by the test particle method mentioned in subsection 2.2.1. The nuclear reaction network contains 250 species (see Table 2). We add some species around ^{44}Ti to Hashimoto's network that contains 242 nuclei (Hashimoto et al. 1989), although it turned out that the result was not changed essentially by the addition.

3. RESULTS

First, initial density structure in our simulation is shown in Fig. 1. This model is the $9.15M_\odot$ collapsar model from MacFadyen and Woosley (1999). The mass of the central black hole is 3.762 $M_\odot$ (Aloy et al. 2000). The surface of this helium star is $R_* = 2.98 \times 10^{10}$ cm. The color represents the density (g cm^{-3}) in logarithmic scale. The polar axis represents the rotation axis, while the horizontal axis represents the equatorial plane. The axis is written in units of cm. The arrows represent the velocity field in (r,θ) plane. The region within 10^{10} cm is shown in the left panel, while that within 10^9 cm is shown in the right panel. An accretion disk is clearly seen in the right panel. The typical specific angular momentum is $\sim 10^{17}$ cm s^{-1} (MacFadyen & Woosley 1999), although this is not shown in Fig. 1.

As explained in section 2.1.2, we deposit thermal energy to launch a jet from the central region of the collapsar. The density structure for Models E51, E52, and E52s at $t = 1.0$ sec (left panel) and $t = 1.5$ sec (right panel) are shown in Figs. 2, 3, and 4. It is clearly shown that a sharp, narrow jet propagates along to the rotation axis in Model E51, which is similar to Aloy et al. (2000). On the other hand, in the case of E52, a broad, deformed shock wave propagates in the progenitor. Also, in Model E52S, the shock wave is deformed even though the thermal energy is deposited in a spherically symmetric way. This is due

to the asymmetry of the density structure of the progenitor. That is, in the low density region around the rotation axis, the injected thermal energy is mainly shared with electrons, positrons, and photons. On the other hand, at the high density region around the equatorial plane, the injected energy is shared with radiations mentioned above and nuclei/nucleons. As a result, the pressure gradient at the energy-injected region becomes aspherical, which causes a bi-polar flow along to the rotation axis. It is also noted that the shock wave is more deformed in Model E52S than Model E52. This will be because the energy density around polar region is higher in Model E52, making this region expands very strongly.

Forms of the mass cut (the boundary between ejecta and the matter that falls into the central black hole) are shown in Fig. 5 for each model. Red particles represent the ones that can escape from the gravitational potential to infinity, while green particles represent the ones that are trapped into the gravitational potential. For a criterion to judge whether a test particles can escape or not, we calculated the total energy (summation of kinetic energy, thermal energy, and gravitational energy) of the test particles at the final stage of simulations ($t = 10$ sec). We judge that a test particle can escape if its total energy is positive, and vice versa.

Strictly speaking, we have to simulate much longer time to determine whether a test particle can really escape or not. In particular, there is a region around the equatorial plane ($r \geq 10^{10}$ cm, $\theta \geq 70^{\circ}$) where shock wave does not reach even at the final stage of the simulations ($t = 10$ sec), because the speed of propagation of the shock wave is slower around the equatorial plane compared with the polar region. In this study, we assumed that such a region where the shock wave does not reach even at the final stage can escape to infinity. This is because such a region is distant from the central black hole ($r \geq 10^{10}$ cm), so gravitational potential is shallow. Moreover, as shown later, at such a distant region, explosive nucleosynthesis hardly occurs and the most important nuclei in this study, ^{56}Ni, is not synthesized. So our results on the abundance of ^{56}Ni do not depend on this assumption.

To show how test particles are ejected clearly, we show the positions of the test particles at $t = 0$ sec (upper left panel of Fig. 6), 3.11 sec (upper right panel of Fig. 6), 3.69 sec (lower left panel of Fig. 6), and 4.27 sec (lower right panel of Fig. 6) for Model E51. The particles colored green, red, and blue are the ones that are put around the rotation axis initially ($\theta \leq 30^{\circ}$), middle range ($30^{\circ} \leq \theta \leq 60^{\circ}$), and equatorial plane ($60^{\circ} \leq \theta \leq 90^{\circ}$), respectively. Radius of the progenitor is 2.98×10^{10} cm. The (white) region where no test particle exist shows the shocked, low density region. It is clearly shown that some fraction of the matter behind the shock wave composes the jet component around the rotation axis, while some fraction of it is pushed sideways toward the θ-direction, which we call as supernova (SN) component in this study. We define the jet component as the matter within the 10° cone

around the rotation axis at the final stage of the calculation, and the rest we define as SN component. The motions of test particles in Models E52 and E52S are similar to Model E51.

Before we show the results of explosive nucleosynthesis, we present contour of entropy per baryon in units of Boltzmann constant (k_b) for Model E51 at $t = 1.5$ sec in the left panel of Fig. 7. For comparison, positions of test particles at that time is shown in the right panel of Fig. 7. As for the entropy per baryon, the range $10^0 - 10^5$, which corresponds to the shocked region, is shown. It is clearly shown that test particles in the downstream of the shock wave are moving with shock velocity, and no test particles are left inside of the shocked region where entropy per baryon is quite high.

We can know where and how much ^{56}Ni is synthesized by doing post processing. Also, we can see how ^{56}Ni is ejected, that is, how much ^{56}Ni is ejected as jet component or SN component. In Fig. 8, positions of the ejected test particles for Model E51 at $t = 0$ sec (left panel) and $t = 4.27$ sec (right panel) are shown that satisfy the condition that the mass fraction of ^{56}Ni becomes greater than 0.3 as a result of explosive nucleosynthesis. Total ejected mass of ^{56}Ni becomes $0.0439 M_\odot$. In particular, total mass of it in the SN component is $0.0175 M_\odot$, which is much smaller than the observed values of hypernovae. In Figs. 9 and 10, same figures with Fig. 8 but for Model E52 and E52S are shown. As mentioned above, the outflow becomes bi-polar due to the asymmetry of density structure. As a result, jet component can be seen even in Model E52S (Fig. 10). Total ejected mass of ^{56}Ni is $0.23 M_\odot$ (Model E52), which is comparable to the observed values of hypernovae. It is also noted that most of the synthesized ^{56}Ni is in the jet component ($0.23 M_\odot$), while small amount of ^{56}Ni ($0.00229 M_\odot$) is in the SN component. From this result, we can guess that some fraction of gamma-ray lines from ^{56}Ni decays appear without losing their energies. This point is discussed in section 4 in detail. Of course, it is noted this model will not explain association of GRBs with hypernovae since this model can not cause highly relativistic jets. The features of Model E52S are same with E52. That is, the ejected mass of ^{56}Ni in Model E52S is $0.28 M_\odot$, which is comparable to Model E52 and is much larger than Model E51. From this result, it is shown that the total ejected mass of ^{56}Ni depends sensitively on the energy deposition rate, and depends not so sensitively on the mass of the heated region (energy-injection region), which is consistent with Nagataki et al. (2003). The reason is as follows: The criterion for the complete silicon burning is $T_{\rm max} \geq 5 \times 10^9$ [K] (Thielemann et al. 1996). It is well known that the matter behind the shock wave is radiation dominated and $T_{\rm max}$ can be estimated well by equating the supernova (hypernova) energy with the radiation energy inside the radius r of the shock front

$$E_{\rm HN} = 10^{52} \left(\frac{E_{\rm HN}}{10^{52} {\rm erg}} \right) = \frac{11\pi^3}{45} \frac{k_b^4}{\hbar^3 c^3} r^3 T_{\rm max}^4 \quad [{\rm erg}], \tag{4}$$

where $E_{\rm HN}$ is the total explosion energy of a hypernova, $\hbar$ is the Planck constant divided by

2π, c is speed of light. Here spherical explosion is assumed. This equation gives r as

$$r = 5.7 \times 10^8 \left(\frac{5 \times 10^9 \mathrm{K}}{T_{\max}} \right)^{4/3} \left(\frac{E_{\mathrm{HN}}}{10^{52} \mathrm{erg}} \right)^{1/3} \quad [\mathrm{cm}]. \tag{5}$$

In the case of Model E52S, ^{56}Ni is synthesized within the edge for the complete silicon burning ($\sim 6 \times 10^8$ cm, see left panel of Fig. 10). The situation should be almost same in the jet-induced explosion Models (Model E52, see left panel of Fig. 9). On the other hand, in the case of Model E51, matter starts to move outwards after the passage of the shock wave, and almost all of the matter move away ($r \geq 6 \times 10^8$ cm) before the injection of thermal energy ($= 10^{52}$ erg) is completed. This is the reason why abundance of ^{56}Ni is little in Model E51. As mentioned above, ^{56}Ni is synthesized within $r \leq 10^9$ cm. So we can conclude that the amount of ^{56}Ni does not depend on the assumption that the region ($\geq 10^{10}$ cm) where the shock wave does not reach even at the final stage of calculation ($t = 10$ sec) can escape to infinity. It should be noted that the chemical composition in the jet is not unchanged for the matter located at $r \geq 10^9$ cm initially. So helium layer and outer oxygen layer located at $r \geq 10^9$ cm are ejected as a jet with chemical composition unchanged.

We have calculated the abundance of heavy elements in the ejecta, using the mass cut and post processing mentioned above. The result is shown in Table 3. Abundances are written in units of $M_\odot$. All unstable nuclei produced in the ejecta are assumed to decay to the corresponding stable nuclei. The amount of ^{56}Ni is also shown in the last row. As explained above, the amount of ^{56}Ni does not depend on the assumption that the region where the shock wave does not reach even at the final stage can escape to infinity. However, the amounts of light elements such as ^{16}O and ^{4}He depends on this assumption, because the progenitor is composed of such light elements. So we think further study should be required to estimate the abundance of light elements ejected from a collapsar more precisely. The abundance of heavy elements in the ejecta normalized by the solar value (Anders & Grevesse 1989; Nagataki 1999) is shown in Fig. 11. Models E51 (black) and E52 (white) are shown in the left panel, while Models E52S (black) and E52 (white) are shown in the right panel. We can see that there is an enhancement of nuclei whose mass number ~ 40 in Models E52 and E52S. This is the result of incomplete silicon burning and alpha-rich freezeout (Nagataki et al. 1997; Nagataki et al. 1998b; Nagataki 2000; Maeda et al. 2002; Maeda & Nomoto 2003).

4. DISCUSSION

First, we discuss the formation of highly relativistic jets to realize GRBs. Of course, in the present study, we can not investigate the acceleration of the jet to relativistic regime

since our numerical code is Newtonian. So we have to investigate this topic using relativistic hydrodynamic code. At present, we discuss this topic by introducing previous works that investigate GRB jets using relativistic hydrodynamic code. Aloy et al. (2000) performed such a calculation using the collapsar model (MacFadyen & Woosley 1999). They have shown that the jet is formed as a consequence of an assumed energy deposition rate in the range of $10^{50} - 10^{51}$ erg s^{-1} within a 30° cone around the rotation axis, which is similar treatment of Model E51 in this study. They reported that the maximum Lorentz factor of the jet becomes 44, which seems to be smaller than required value to explain GRBs (~ 300; Piran 1999). Zhang et al. (2003) also calculated propagation of the relativistic jet through the collapsar with constant energy deposition rate $10^{50} - 3 \times 10^{50}$ erg s^{-1}. They set the location of the inner boundary to be 2×10^8 cm. They estimated terminal Lorentz factor, which is calculated by assuming that all internal energy is converted into kinetic energy, becomes $\sim$100, although their calculated Lorentz factor of the jet is $\sim$50 at most. Zhang and Woosley (2004) have improved their code and demonstrated that the bulk Lorentz factor of the jet can reach $\sim$100, although they set the inner boundary to be 10^{10} cm. From their works, we can understand it very difficult to realize a highly relativistic jet whose bulk Lorentz factor becomes larger than 100. They required a collimated, narrow jet by depositing explosion energy for ~ 10 sec. The importance of the collimation to realize a highly relativistic jet can also be understood by rough estimation. We can calculate the mass of the progenitor included within a cone around the rotation axis. The masses included within a cone with the zenith angles $3°, 5°, 10°, 15°$ are $7.9 \times 10^{30}, 3.1 \times 10^{31}, 7.1 \times 10^{31}, 2.0 \times 10^{32}$ g, respectively. So if these matter are accelerated to highly relativistic regime with bulk Lorentz factor Γ, the kinetic energies have to be $7.1 \times 10^{53}(\Gamma/100), 2.8 \times 10^{54}(\Gamma/100), 6.4 \times 10^{54}(\Gamma/100), 1.8 \times 10^{55}(\Gamma/100)$ erg, respectively, which shows the importance of collimation. The importance of collimation is also confirmed by our forth-coming paper (Mizuta et al. 2006). In Models E52 and E52S, the opening angles of the jets are wider than that in Model E51 (see Figs. 2,3,4), so we consider that highly relativistic jet will not be produced in Models E52 and E52S even if relativistic hydrodynamic code is used. So we consider that Models E52 and E52S can not explain the phenomena of association of GRBs with hypernovae, even though much ^{56}Ni is synthesized in these models.

There is another question. Does all of ^{56}Ni produced in the jet of the collapsar model brighten the supernova remnant? If the jet becomes optically thin before ^{56}Ni decays into ^{56}Co and ^{56}Co decays into ^{56}Fe, these nuclei should result in only emitting gamma-rays and can not brighten the supernova remnant. Colgate et al. (1980) consider the deposition of energy by gamma-rays emanating from decay of ^{56}Ni and ^{56}Co. They found that the mass opacity of the gamma-ray absorption is about 0.029 cm^2 g^{-1}, for either ^{56}Ni or ^{56}Co decay spectrum. The half-lives of ^{56}Ni and ^{56}Co are 5.9 and 77.1 days. So we can roughly estimate

the opacity for these gamma-rays in the jet. We assume that the opening angle of the jet is 10° and expansion velocity of the jet is speed of light. Under these assumption, when substantial ^{56}Ni decays into ^{56}Co, the volume of the jet becomes $3.2 \times 10^{-2} R^3$ cm^3, where R is the radius of the jet with $R = 1.5 \times 10^{16}\Gamma$ cm and Γ is the bulk Lorentz factor of the jet. Since the mass included within a cone with the zenith angles 10° is 7.1×10^{31} g, the density of the jet at that time becomes 6.6×10^{-16} g cm$^{-3}\Gamma^{-3}$. So the mean free path of the gamma-rays becomes $5.3 \times 10^{16}\Gamma^3$ cm, which is comparable or longer than the radius of the jet. Of course, the gamma-rays can easily escape from the side of the cone. So we think most of the gamma-rays produced in a jet will escape without depositing energy to the jet and supernova components as long as the bulk speed of the jet is relativistic. Similar discussion can be adopted for the decays of ^{56}Co into ^{56}Fe. So, we can conclude that some fraction of gamma-ray lines from ^{56}Ni decays in the jet may appear as gamma-rays, which may be observed as relativistically Lorentz boosted gamma-ray line profiles in future. To obtain more firm conclusion, it will be necessary to perform multi-dimensional relativistic hydrodynamics with radiation transfer and calculate the light curve of hypernovae.

Here we have to make a comment on the resolution of numerical simulations in this study. It is shown in numerical simulations with high resolution (Zhang & Woosley 2004) that the jet propagates only mildly relativistically ($\sim$c/2) while in the star, and shocked gas can move laterally to form a cocoon, allowing the core of the jet to remain relativistic. Thus the total mass accelerated relativistically ($\Gamma \sim 100$) by the jet is not the fraction of the star intercepted by the jet, although the importance of collimation can be understood by calculating mass within the cone of the jet as mentioned above. So, strictly speaking, there are three components in a collapsar model, highly relativistic jet, cocoon, and supernova component when relativistic hydrodynamic simulations are performed. In this study, highly relativistic jet and cocoon are called as 'jet component'.

We concluded that the highly relativistic jet and mildly relativistic cocoon are optically thin against the gamma-rays that come from decays of ^{56}Ni and ^{56}Co. As mentioned above, mean free path of the gamma-rays becomes $5.3 \times 10^{16}\Gamma^3$ cm, which is comparable or longer than the radius of the jet component, $1.5 \times 10^{16}\Gamma$ cm (Note that these are comparable even if $\Gamma = 1$). So the ^{56}Ni in the highly relativistic jet and mildly relativistic cocoon should not contribute to the light curve of a supernova. On the other hand, sub-relativistic cocoon will be optically thick against the gamma-rays. So sub-relativistic cocoon may have contribution to the optical light curve of hypernovae. In fact, it is clear that too much energy is required to accelerate all of ^{56}Ni in the jet to relativistic speed. From the discussion of energetics mentioned above, the required energy (erg) becomes $9.0 \times 10^{53}(\Gamma/1)(M_{\rm Ni}/0.5M_\odot)$ where $M_{\rm Ni}$ is the mass of ^{56}Ni. Thus we consider that there is a possibility that a part of the gamma-ray lines may appear without losing their energies. As mentioned above, numerical simulations

of relativistic hydrodynamics with high resolution should be required to distinguish highly relativistic jet from cocoon, and to obtain precise distribution of burning products, which we are planning to simulate in near future.

Let us emphasize our motivation in this work here. In this study, we want to consider the consistency between the collapsar model of MacFadyen and Woosley (1999) and explosive nucleosynthesis in a hypernova jet. The answer is as follows. From the discussions mentioned above, it seems difficult to explain the required amount of ^{56}Ni ($\sim 0.5 M_{\odot}$) by the explosive nucleosynthesis in the jet. We think the another idea that the origin of ^{56}Ni is the explosive nucleosynthesis in the accretion disk (MacFadyen & Woosley 1999; Pruet et al. 2002) is much simpler and adequate to explain the association of GRBs and hypernovae. In this scenario, it is not necessary for ^{56}Ni to be synthesized in a short timescale as Models E52 and E52S. As explained in section 1, in the collapsar scenario, the jet is launched ~ 7 sec after the gravitational collapse and the duration of the jet is about 10 sec, which is much longer than the typical timescale of normal core-collapse supernovae and comparable to the typical observed duration of GRBs. As a result of gravitational collapse in a long timescale, the density around the rotation axis becomes low, which is a good environment to produce a fire ball. That is, long timescale of the order of 10 sec is essential to realize a GRB. As shown in this study, in such a case (Model E51), ^{56}Ni is not synthesized so much in the jet. Rather, it will be natural to consider that the origin of ^{56}Ni is the accretion disk around the black hole. In this scenario, ^{56}Ni is also ejected in a long timescale of the order of 10 sec. No requirement that ^{56}Ni has to be produced in a short timescale exists in this scenario. Also, as shown in this study, the explosion becomes naturally bi-polar in any case (even in Model E52S) due to the aspherical density structure of the progenitor. So it will be natural to consider that the ^{56}Ni synthesized in the accretion disk and conveyed as outflows are blown along to the rotation axis, which can explain the line features of SN 1998bw and double peaked line features of SN 2003jd (Mazzali et al. 2005). Of course, there is much uncertainty how much ^{56}Ni is ejected from the accretion disk. This problem depends sensitively on the effects of viscosity. Further investigation is required to estimate how much ^{56}Ni is ejected. At present study too, how much ^{56}Ni is ejected from the accretion disk is not estimated since artifitial viscosity and/or magnetic fields are not included.

It should be noted that there are varieties of observations and theories related with the association of GRBs with supernovae. As a result, it will be natural to consider that there are varieties of explosive nucleosynthesis in the collapsar. For example, there will be a class of 'failed GRBs' (Lazzati et al. 2002; Totani 2003), in which baryon-rich jet propagates. In this class, there is a possibility that much heavy elements are synthesized because of high density in the jet (Inoue et al. 2004), while light elements will be synthesized in baryon-poor jets (Lemoine 2002; Pruet et al. 2002; Beloborodov 2003). Also, if the central engine

of the GRBs is a magnetar (Rees & Mészáros 2000; Takiwaki et al. 2004) or magnetized collapsar (Blandford & Znajek 1977; Blandford & Payne 1982; Proga et al. 2003; Koide 2003; Mizuno et al. 2004; Proga 2005; McKinney 2005a; McKinney 2005b), the timescale of the explosion will be shorter than that of a collapsar, which will result in the different way of nucleosynthesis in this study. Further investigation should still be required to understand the central engine of GRBs and origin of ^{56}Ni in hypernovae.

In the early universe, where the metal content of gas is very low, the enrichment by a single supernova can dominate the preexisting metal contents (Audouze & Silk 1995). Since GRBs also occurs from the early universe, there is a possibility that some fraction of metal poor star reflects the chemical abundance of GRBs accompanied by hypernovae (Maeda & Nomoto 2003). From Fig. 11, we can see that there is an enhancement of nuclei whose mass number ~ 40 in Models E52 and E52S compared with Model E51. This is the result of incomplete silicon burning and alpha-rich freezeout (Nagataki et al. 1997; Nagataki et al. 1998b; Nagataki 2000; Maeda et al. 2002; Maeda & Nomoto 2003). In particular, in Models E52 and E52S, $[\mathrm{Ca/Si}] \equiv \log(X_{\mathrm{Ca}}/X_{\mathrm{Si}}) - \log(X_{\mathrm{Ca}}/X_{\mathrm{Si}})_{\odot}$ is larger than unity, where X_i is the mass fraction of the ith element and $(X_{\mathrm{Ca}}/X_{\mathrm{Si}})_{\odot}$ is the solar value, which is in contrast with Model E51 and previous works (Qian & Wasserburg 2002; Pruet et al. 2004). So it may be determined which model is the proper one as a model of hypernova by observations of chemical composition in metal poor stars (Ishimaru & Wanajo 1999; Umeda & Nomoto 2002; Tsujimoto 2004; Ishimaru et al. 2004; Umeda & Nomoto 2005).

It will be a good challenge to perform a calculation of the r-process and/or p-process nucleosynthesis in the GRB jet in this study, because this jet will also be able to realize a high entropy condition enough to realize these processes (MacFadyen & Woosley 1999; Nagataki 2000; Nagataki 2001; Nagataki & Kohri 2001; Wanajo et al. 2002; Suzuki & Nagataki 2005). As shown in Fig. 7, there is really a region in the jet where high entropy per baryon is realized (it reaches to 10^5 at most!). However, in this study, test particles in the downstream of the shock wave are moving with shock velocity, and no test particles are left inside of the shocked region where entropy per baryon is quite high. So other method will be required to investigate the r-process and/or p-process nucleosynthesis in the jet. We are planning to perform such calculations. Results will be presented in near future.

After we have written this manuscript, we found recent papers by Maeda et al. (2005) and Maeda (2005) in which similar topic of this study is considered. Their conclusions are consistent with our prediction. That is, they calculated gamma-ray lines from ^{56}Ni decays in the jet, although relativistically Lorentz boosted line profiles are not calculated because they used a Newtonian code. Also, it is noted that they deposit all explosion energy as an initial condition like Model E52 and E52S in this study. That is why they can obtain enough

^{56}Ni to explain the light curve of SN 1998bw, which is consistent with the results in this study. The reason why they obtained a little more ^{56}Ni ($\sim 0.4 M_{\odot}$) may be the difference of the progenitor. They used a spherically symmetric progenitor while we have used a collapsar model. As stated in this study, the density of the collapsar model around the polar region is lower than the spherically symmetric progenitor. So the abundance of synthesized ^{56}Ni may be smaller in this study.

5. SUMMARY AND CONCLUSION

We have performed 2-dimensional hydrodynamic simulations to investigate explosive nucleosynthesis in a collapsar using the model of MacFadyen and Woosley (1999). We have shown that ^{56}Ni is not produced in the jet sufficiently to explain the observed amount of a hypernova such as SN 1998bw when the duration of the explosion is $\sim$10 sec (the standard model, E51). Even though a considerable amount of ^{56}Ni is synthesized if all explosion energy is deposited initially (the extreme models, E52 and E52S), the opening angles of the jets become too wide to realize highly relativistic outflows and a GRB in such a case. From these results, it is concluded that the origin of ^{56}Ni in hypernovae associated with GRBs is not the explosive nucleosynthesis in the jet. We consider that the idea that the origin of ^{56}Ni in hypernovae is the explosive nucleosynthesis in the accretion disk is more promising. We have also shown that the explosion becomes bi-polar naturally due to the effect of the deformed progenitor. This fact suggests that the ^{56}Ni synthesized in the accretion disk and conveyed as outflows are blown along to the rotation axis, which will explain the line features of SN 1998bw and double peaked line features of SN 2003jd, and will help the idea of the accretion disk mentioned above.

Also, some predictions are presented in this study. Some fraction of the gamma-ray lines from ^{56}Ni decays in the jet will appear without losing their energies because the jet becomes optically thin before a considerable amount of ^{56}Ni decays as long as the jet is a relativistic flow. So it has been predicted that some fraction of ^{56}Ni synthesized in the jet may show relativistically Lorentz boosted line profiles. That is, highly blue shifted (or red shifted) broad line features might be observed in future. It has been also shown that there is an enhancement of nuclei whose mass number ~ 40 in Models E52 and E52S compared with Model E51 as a result of incomplete silicon burning and alpha-rich freezeout. So it may be determined which model is the proper one as a model of a gamma-ray burst accompanied by a hypernova by observations of chemical composition in metal poor stars.

Of course there is still uncertainty of observations and theories on the formation of GRBs accompanied by hypernovae. Further investigation should still be required to understand

the central engine of GRBs and origin of ^{56}Ni in hypernovae.

We are grateful to the anonymous referee of this paper for fruitful comments. We are grateful to A. MacFadyen for giving us a result of numerical simulation of a collapsar and useful discussion. S.N. are also grateful to M. Watanabe and S. Yamada for useful discussion. The computation was partly carried out on NEC SX-5 and SX-8, SGI Altix3700 BX2, and Compaq AlphaServer ES40 at Yukawa Institute for Theoretical Physics, and Fujitsu VPP5000 at National Astronomical Observatory of Japan. This work is in part supported by a Grant-in-Aid for the 21st Century COE "Center for Diversity and Universality in Physics" from the Ministry of Education, Culture, Sports, Science and Technology of Japan. S.N. is partially supported by Grants-in-Aid for Scientific Research from the Ministry of Education, Culture, Sports, Science and Technology of Japan through No. 14102004, 14079202, and 16740134.

REFERENCES

Aloy, M.A., et al., 2000, ApJ, 531, L119

Anders, E., Grevesse, N. 1989, GeCoA, 53, 197

Audouze, J., Silk, J. 1995, ApJ, 451, L49

Beloborodov, A.M. 2003, ApJ, 588, 931

Blandford, R.D., Znajek, R.L. 1977, MNRAS, 179, 433

Blandford, R.D., Payne, D.G. 1982, MNRAS, 199, 883

Blinnikov, S.I., Dunina-Barkovskaya, N.V., Nadyozhin, D.K. 1996, ApJ, 106, 171

Bloom, J.S., et al. 1999, Nature, 401, 453

Bloom, J.S., Kulkarni, S.R., Djorgovski, S.G. 2002, AJ, 123, 1111

Colgate, S.A., Petschek, A.G., Kriese, J.T. 1980, ApJ, 237, L81

Galama, T.J., et al., 1998, Nature, 395, 670

Galama, T.J., et al. 2000, ApJ, 536, 185

Garnavich, P.M., et al. 2003, ApJ, 582, 924

Gorosabel, J. et al. 2003, A&A, 409, 123

Hashimoto, M., Nomoto, K., Shigeyama, T. 1989, A&A, 210, L5

Hjorth, J., et al. 2003, Nature, 423, 847

Inoue, S., Iwamoto, N., Orito, M., Terasawa, M. 2003, ApJ, 595, 294

Ishimaru, Y., Wanajo, S. 1999, ApJ, 511, L33

Ishimaru, Y., Wanajo, S., Aoki, W., Ryan, S.G. 2004, ApJ, 600, L47

Iwamoto, K., et al., 1998, Nature, 395, 672

Khokhlov, A.M., et al. 1999, ApJ, 524, L107

Koide, S. 2003, Phys. Rev. D., 67, 104010

Kotake, K., Yamada, S., Sato, K. 2003, ApJ, 595, 304

Kouveliotou, C. 1993, ApJ, 413, L101

Lamb, D.Q., Graziani, C., Smith, I.A. 1993, ApJ, 420, 171

Lazzati, D., Covino, S., Ghisellini, G. 2002, MNRAS, 330, 583

Lemoine, M. 2002, A&A, 390, L31

MacFadyen, A.I., Woosley, S.E., ApJ, 1999, 524, 262

Maeda, K., et al., 2002, ApJ, 565, 405

Maeda, K., Nomoto, K. 2003, ApJ, 598, 1163

Maeda, K., Mazzali, P.A., Nomodo, K. 2005, astro-ph/0511389

Maeda, K. 2005, astro-ph/0511480

Mazet, E.P., et al. 1981, Ap&SS, 80, 3

Mazzali, P.A., et al. 2001, ApJ, 559, 1047

Mazzali, P.A., et al. 2005, Science, 308, 1284

McKinney, J.C. 2005a, astro-ph/0506368

McKinney, J.C. 2005b, astro-ph/0506369

Mizuno, Y. et al. 2004, ApJ, 606, 395

Mizuta, A. et al. 2006, ApJ, submitted.

Nagataki, S., Hashimoto, M., Sato, K., Yamada, S. 1997, ApJ, 486, 1026

Nagataki, S., Shimizu, T.M., Sato, K. 1998, ApJ, 495, 413

Nagataki, S., Hashimoto, M., Sato, K., Yamada, S., Mochizuki, Y.S. 1998b, ApJ, 492, L45

Nagataki, S. 1999, ApJ, 511, 341

Nagataki, S., 2000, ApJS, 127, 141

Nagataki, S. 2001, ApJ, 551, 429

Nagataki, S., Kohri, K. 2001, PASJ, 53, 547

Nagataki, S., Mizuta, A., Yamada, S. Takabe, H., Sato, K. 2003, ApJ, 596, 401

Paczyński, B., Witta, P.J. 1980, A&A, 88, 23

Piran, T. 1999, Phys. Rep., 314, 575

Price, P.A., et al. 2003, Nature, 423, 843

Proga, D., MacFadyen, A.I., Armitage, P.J., Begelman, M.C. 2003, ApJ, 599, L5

Proga, D. 2005, ApJ, 629, 397

Pruet, J., Guiles, S., Fuller, G.M. 2002, ApJ, 580, 368

Pruet, J., Woosley, S.E., Hoffman, R.D. 2003, ApJ, 586, 1254

Pruet, J., Surman, R., McLaughlin, G.C. 2004, ApJ, 602, L101

Qian, Y.-Z., Wasserburg, G.J. 2002, ApJ, 567, 515

Rees, M.J. 1967, MNRAS, 135, 345

Rees, M.J., Mészáros, P. 2000, ApJ, 545, L73

Reichart, D.E., 1999, ApJ, 521, L111

Rhoads, J.E., 1999, ApJ, 525, 737

Shimizu T.M, Yamada S., Sato K. 1994, ApJ, 432, L119

Stanek, K.Z., et al. 1999, ApJ, 522, L39

Stanek, E.Z. 2003, ApJ, 591, L17

Suzuki, T.K., Nagataki, S. 2005, ApJ, 628, 914

Takiwaki, T., Kotake, K., Nagataki, S., Sato, K. 2004, ApJ, 616, 1086

Thielemann, F.-K., Nomoto, K., & Hashimoto, M., 1996, ApJ, 460, 408

Totani, T. 2003, ApJ, 598, 1151

Tsujimoto, T. 2004, ApJ, 611, L17

Umeda, H., Nomoto, K. 2002, ApJ, 565, 385

Umeda, H., Nomoto, K. 2005, ApJ, 619, 427

Vreeswijk, P.M., 2001, A&A, 380, L21

Wanajo, S., Kajino, T., Mathews, G.J., Otsuki, K. 2001, ApJ, 533, 424

Wanajo, S., Itoh, N., Ishimaru, Y., Nozawa, S., Beers, T.C. 2002, ApJ, 577, 853

Wilson R.B. 1985, in Numerical Astrophysics, p.422, eds. J.M. Centrella, J.M. LeBlanc., R.L. Bowers (Jones & Bartlett: Boston)

Woltjer, L. 1966, ApJ, 146, L597

Woosley, S.E., ApJ, 1993, 405, 273

Woosley, S.E., Eastman, R.G., Schmidt, B.P., 1999, ApJ, 516, 788

Yamada. S., Sato. K., 1994, ApJ, 434, 268

Zhang, W., Woosley, S.E., MacFadyen, A.I. 2003, ApJ, 586, 356

Zhang, W., Woosley, S.E. 2004, ApJ, 608, 365

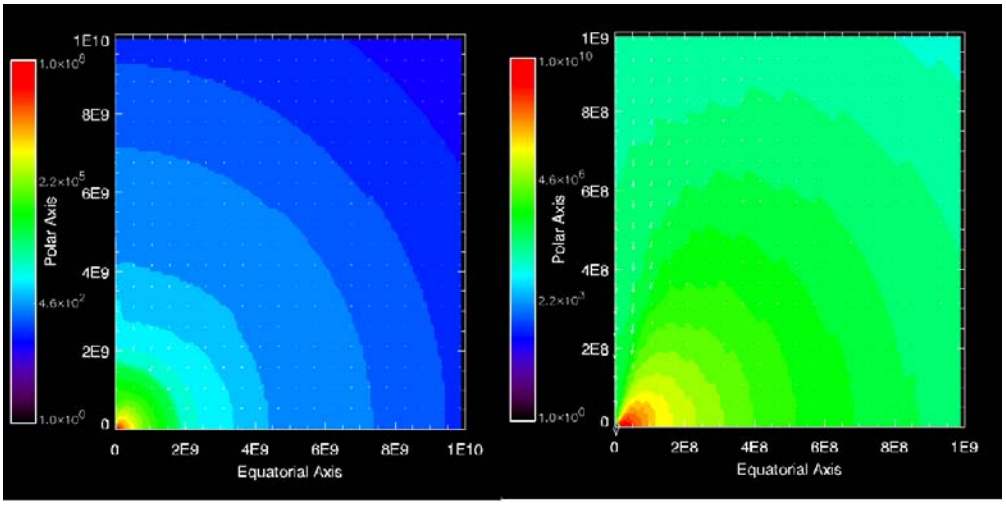

Fig. 1.— Initial density structure in our simulation. This model is the $9.15 M_{\odot}$ collapsar model from MacFadyen and Woosley (1999). The mass of the central black hole is 3.762 $M_{\odot}$. The surface of this helium star is $R_{*} = 2.98 \times 10^{10}$ cm. The color represents the density (g cm^{-3}) in logarithmic scale. The polar axis represents the rotation axis, while the horizontal axis represents the equatorial plane. The axis is written in units of cm. The arrow represents the velocity field in (r,θ) plane. The region within 10^{10} cm is shown in the left panel, while that within 10^{9} cm is shown in the right panel.

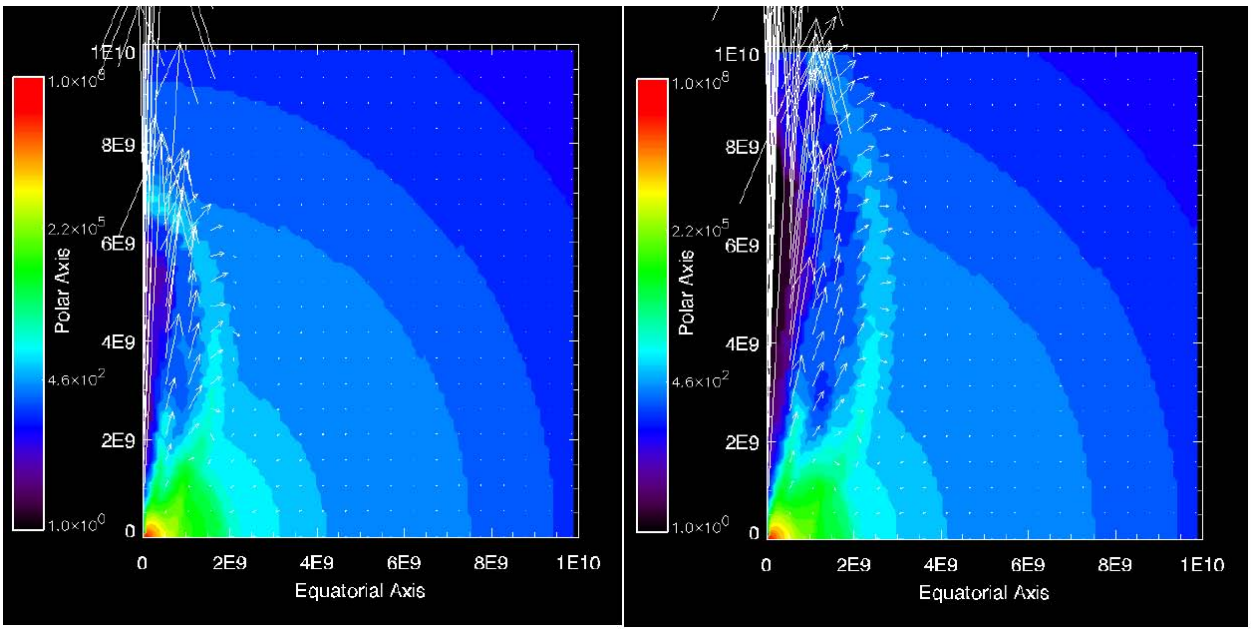

Fig. 2.— Density structure and velocity field of Model E51 at t = 1.0 sec (left panel) and t = 1.5 sec (right panel).

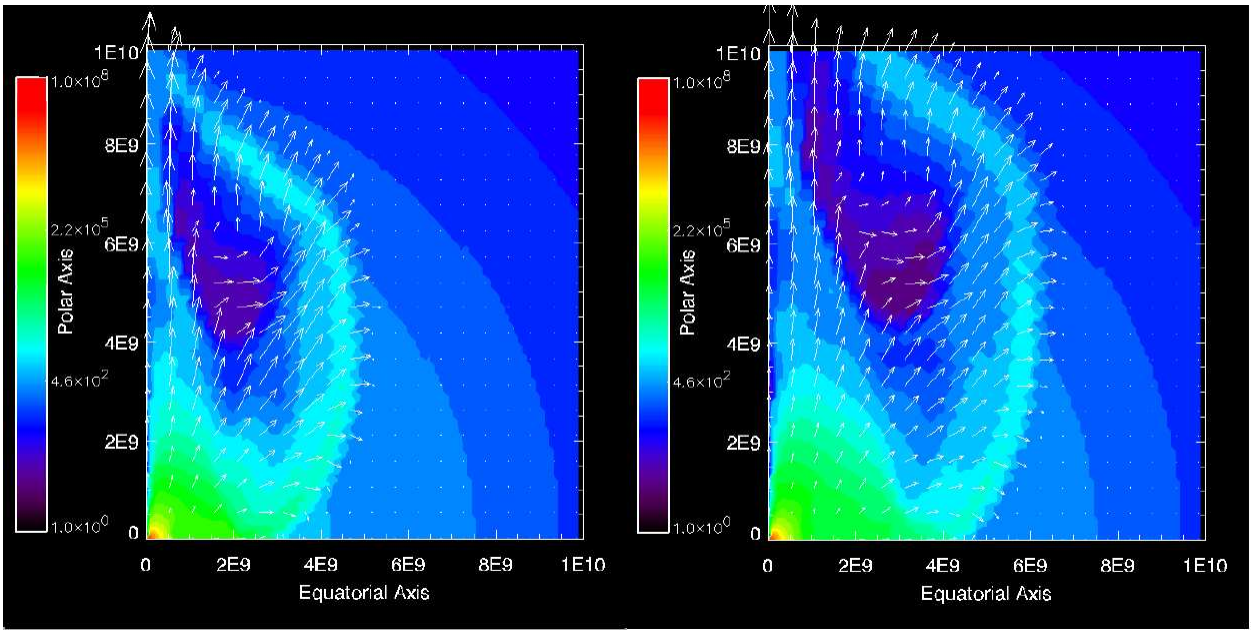

Fig. 3.— Same with Fig. 2, but for the Model E52 at t = 1.0 sec (left panel) and t = 1.5 sec (right panel).

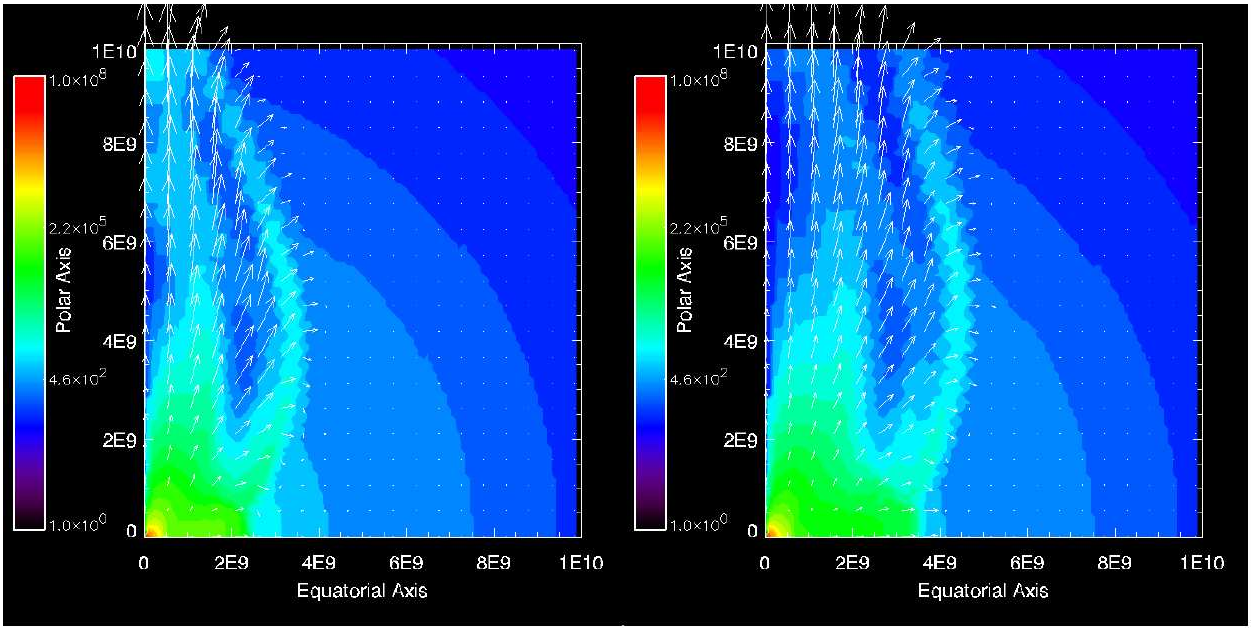

Fig. 4.— Same with Fig. 2, but for the Model E52s at t = 1.0 sec (left panel) and t = 1.5 sec (right panel). It is clearly shown that the shock wave is deformed even though the thermal energy is deposited in a spherically symmetric way as an initial condition. This is due to the asymmetry of the density structure of the progenitor.

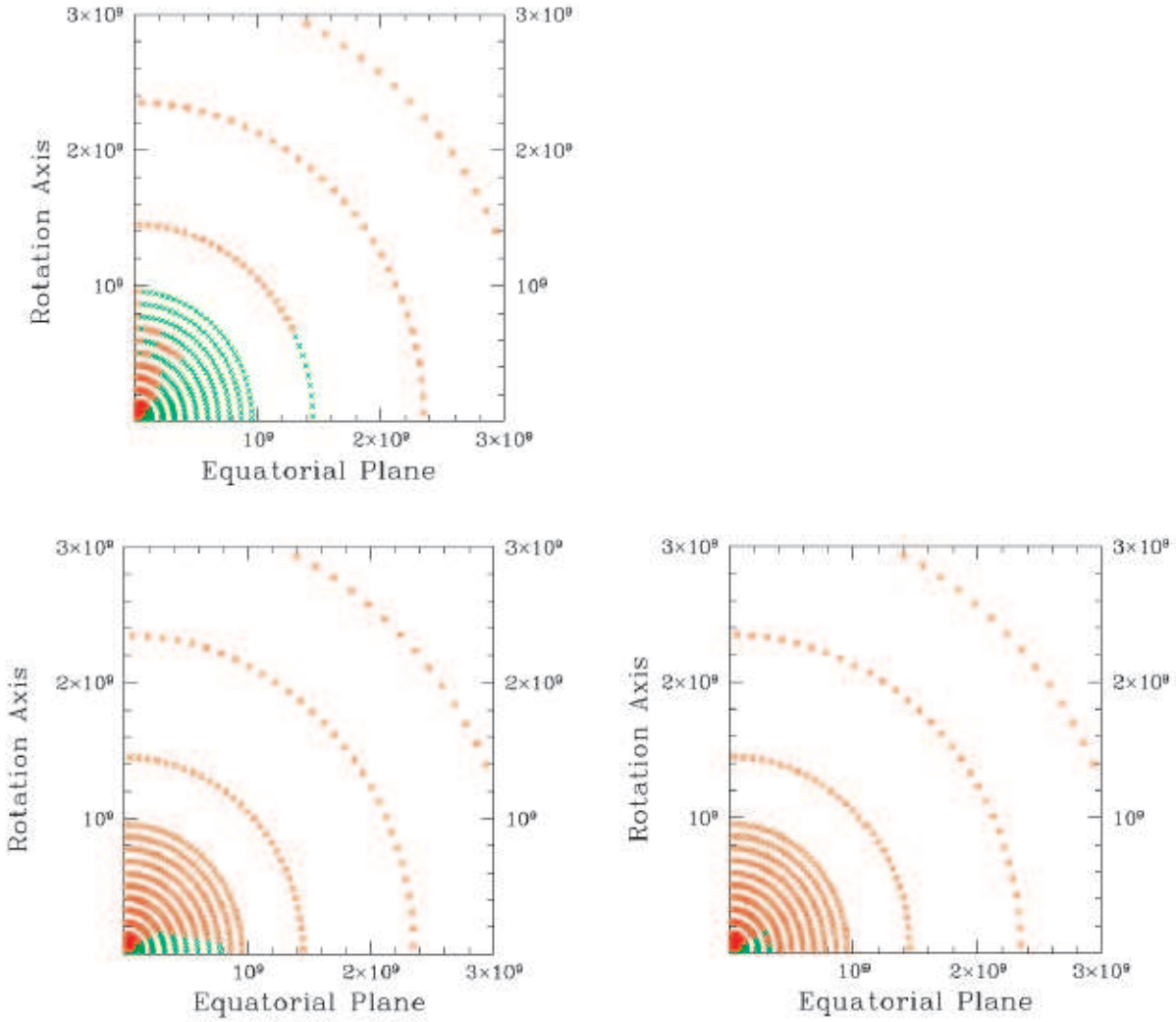

Fig. 5.— Mass cut for the Model E51 (upper panel), Model E52 (lower left panel), and Model E52S (lower right panel). Red particles represent the ones that can escape from the gravitational potential to infinity, while green particles represent the ones that are trapped into the gravitational potential.

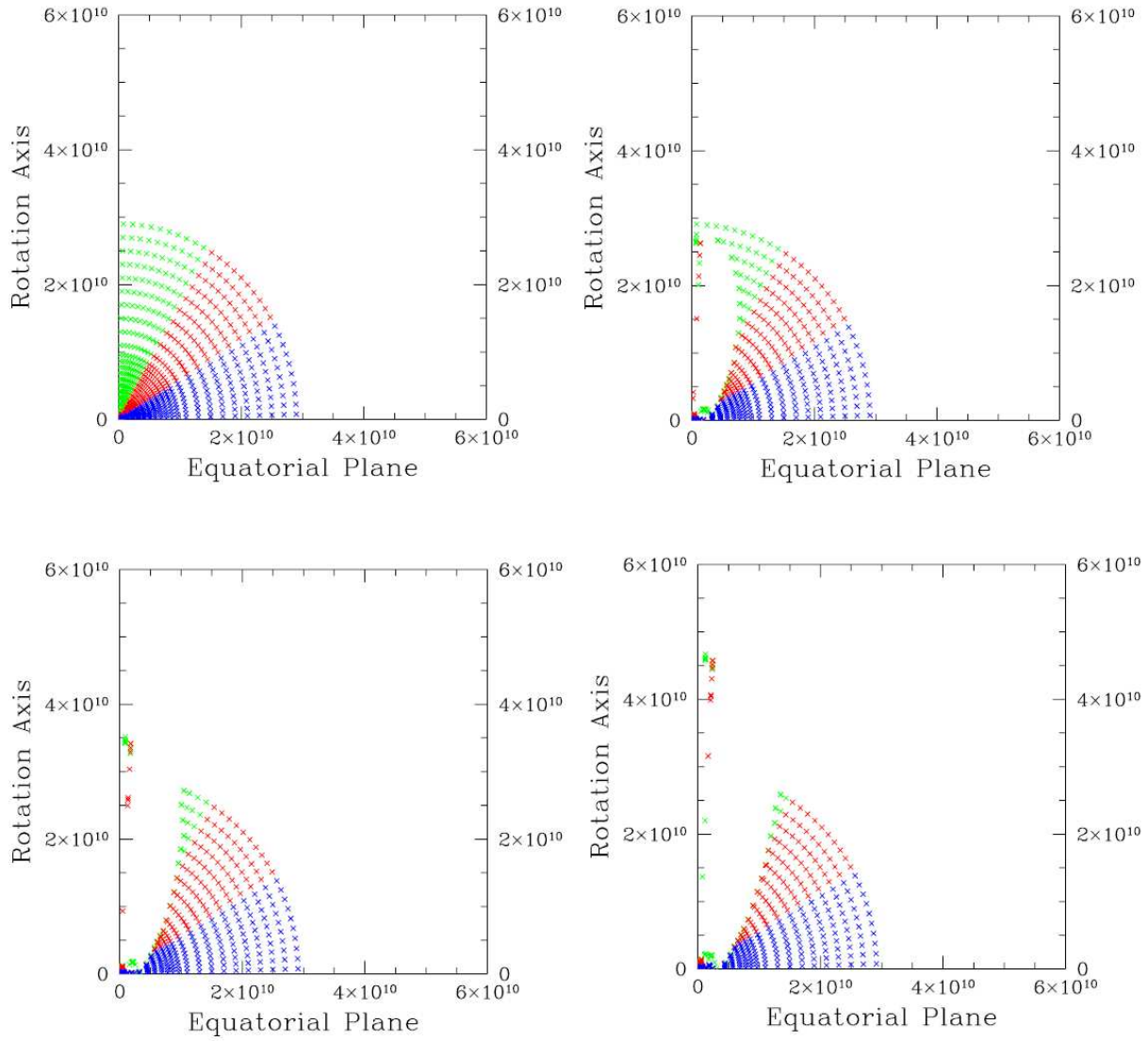

Fig. 6.— Positions of test particles at $t = 0$ sec (upper left panel), $t = 3.11$ sec (upper right panel), $t = 3.69$ sec (lower left panel), and $t = 4.27$ sec (lower right panel) for Model E51. The particles colored green, red, and blue are the ones that are put around the rotation axis initially ($\theta \leq 30°$), middle range ($30° \leq \theta \leq 60°$), and equatorial plane ($60° \leq \theta \leq 90°$), respectively, where θ is the zenith angle. Radius of the progenitor is 2.98×10^{10} cm. The (white) region where no test particle exist shows the shocked, low density region. It is clearly shown that some fraction of the matter behind the shock wave composes the jet component around the rotation axis, while some fraction of it is pushed away toward the θ-direction that composes supernova component.

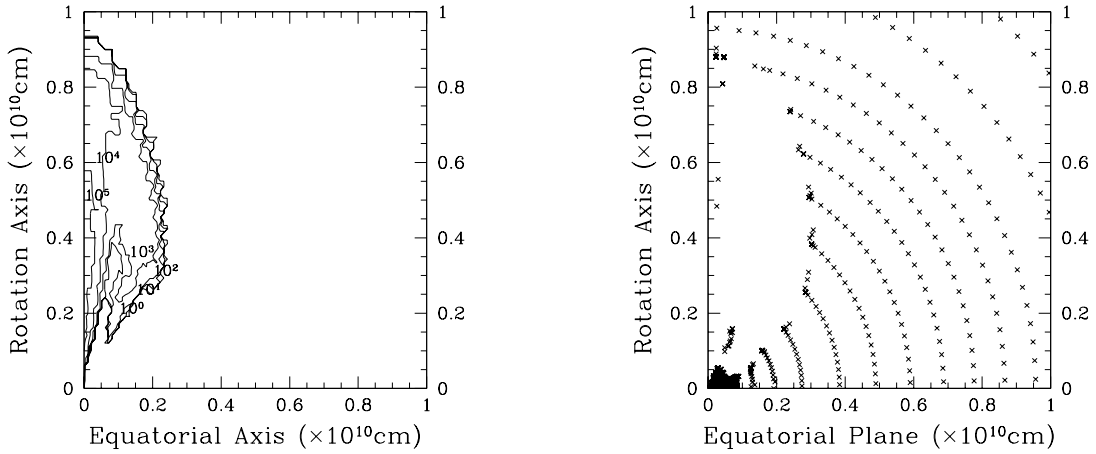

Fig. 7.— Left panel: contour of entropy per baryon in units of k_b for Model E51 at $t = 1.5$ sec. Right panel: positions of test particles for Model E51 at $t = 1.5$ sec. As for the entropy per baryon, the range $10^0 - 10^5$, which corresponds to the shocked region, is shown. It is clearly shown that test particles in the downstream of the shock wave are moving with shock velocity, and no test particles are left inside of the shocked region where entropy per baryon is quite high.

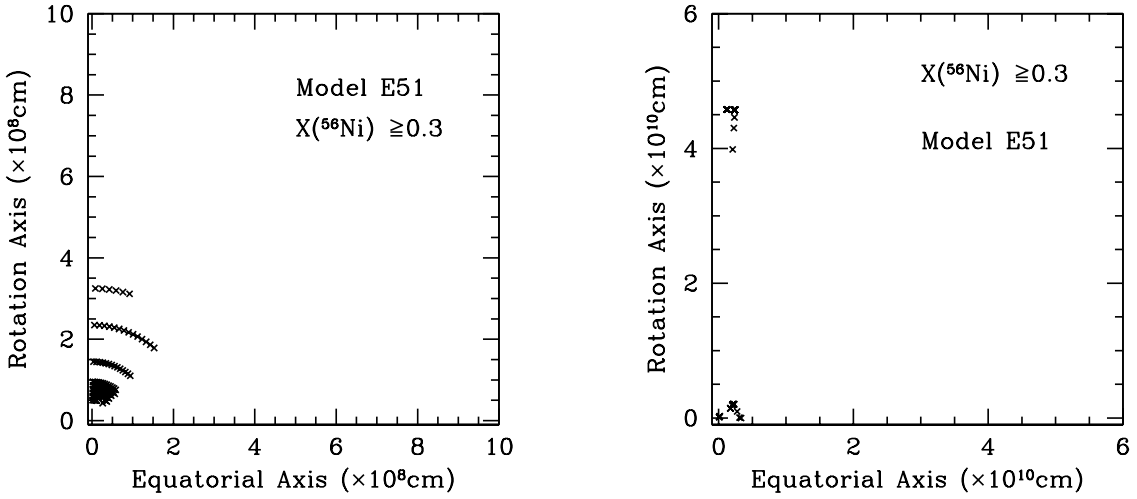

Fig. 8.— Positions of the ejected test particles at $t = 0$ sec (left panel) and $t = 4.27$ sec (right panel) that meet the condition that the mass fraction of ^{56}Ni becomes greater than 0.3 as a result of explosive nucleosynthesis for Model E51 . Total ejected mass of ^{56}Ni becomes $0.0439 M_{\odot}$. In particular, total mass of it in the supernova component is $0.0175 M_{\odot}$, which is much smaller than the observed value of hypernovae.

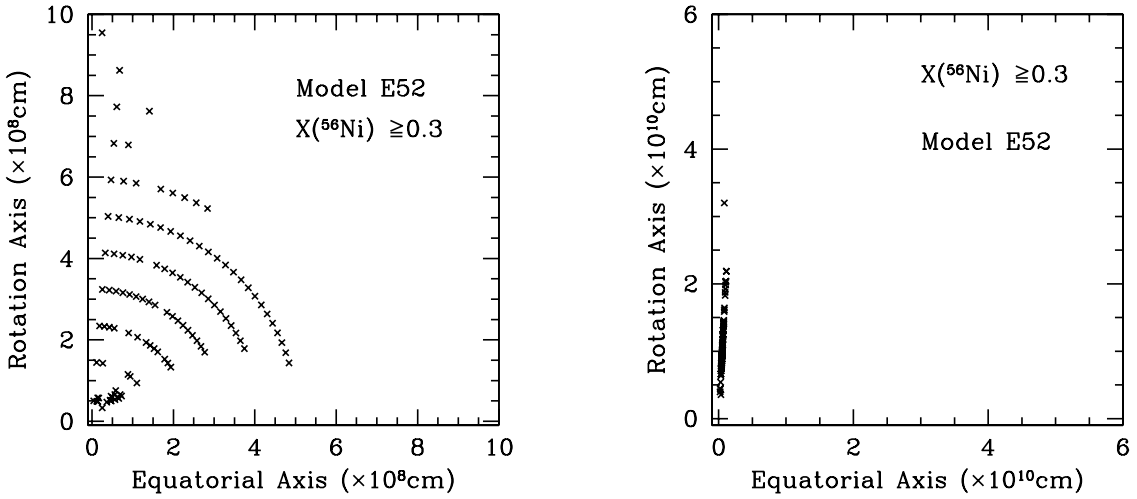

Fig. 9.— Same with Fig. 8, but for Model E52. Total ejected mass of ^{56}Ni is $0.23 M_{\odot}$ (Model E52), which is comparable to the observed value of hypernovae. However, most of the synthesized ^{56}Ni is in the jet component ($0.23 M_{\odot}$), while small amount of ^{56}Ni ($0.00229 M_{\odot}$) is in the supernova component.

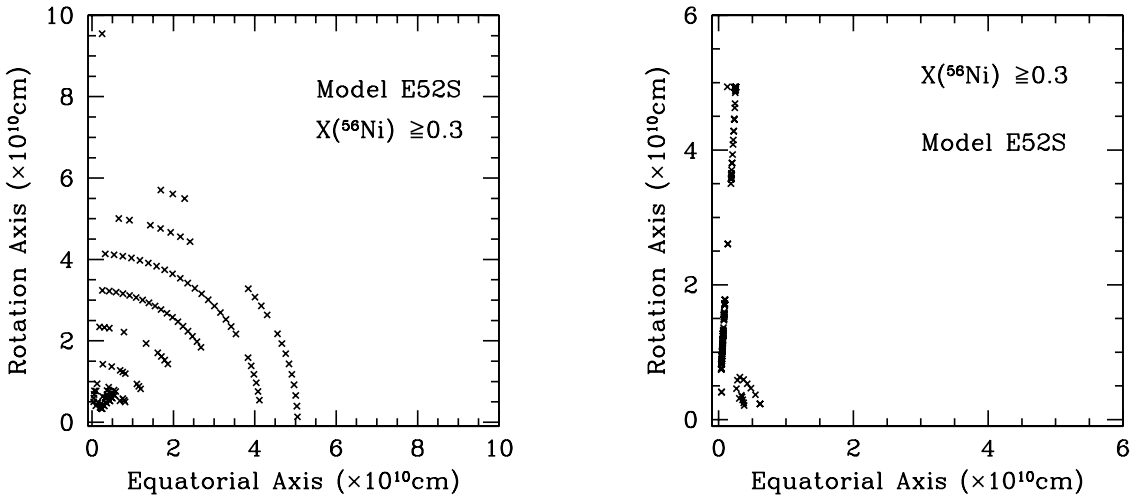

Fig. 10.— Same with Fig. 8, but for Model E52s (right panel). Total ejected mass of ^{56}Ni is $0.28M_{\odot}$ (Model E52s), respectively, which is comparable to the observed value of hypernovae. However, as Model E52, most of the synthesized ^{56}Ni is in the jet component ($0.195M_{\odot}$), while small amount of ^{56}Ni ($0.0882M_{\odot}$) is in the supernova component.

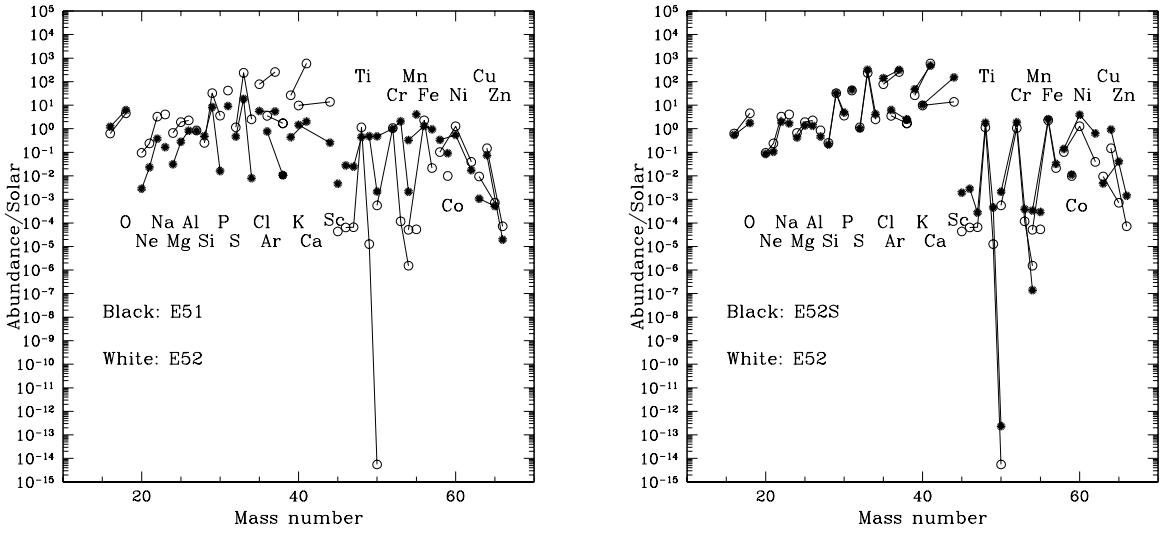

Fig. 11.— Abundance of heavy elements in the ejecta normalized by the solar value. All unstable nuclei produced in the ejecta are assumed to decay to the corresponding stable nuclei. Models E51 (black) and E52 (white) are shown in the left panel while Models E52S (black) and E52 (white) are shown in the right panel.

Model	$\theta_{\rm Jet}$	$\dot{E}$ [erg s^{-1}]	$E_{\rm tot}$ [erg]
E51	30°	10^{51}	10^{52}
E52	30°	∞	10^{52}
E52S	90°	∞	10^{52}

Table 1: Models, half-angle of the initial jet, thermal energy deposition rate, and total explosion energy.

Element	$A_{\rm min}$	$A_{\rm max}$	Element	$A_{\rm min}$	$A_{\rm max}$	Element	$A_{\rm min}$	$A_{\rm max}$
N	1	1	Al	24	30	V	44	54
H	1	1	Si	26	33	Cr	46	55
He	4	4	P	28	36	Mn	48	58
C	11	14	S	31	37	Fe	52	61
N	12	15	Cl	32	40	Co	54	64
O	14	19	Ar	35	45	Ni	56	65
F	17	22	K	36	48	Cu	58	68
Ne	18	23	Ca	39	49	Zn	60	71
Na	20	26	Sc	40	51	Ga	62	73
Mg	22	27	Ti	42	52	Ge	64	74

Table 2: Nuclear Reaction Network Employed

Species	E51	E52	E52S	Species	E51	E52	E52S
^{16}O	3.38E-01	5.27E-01	5.01E-01	^{45}Sc	7.33E-09	3.61E-10	1.96E-08
^{18}O	3.93E-03	8.62E-03	3.66E-03	^{46}Ti	1.79E-07	1.25E-09	6.01E-08
^{20}Ne	1.33E-04	1.34E-02	1.30E-02	^{47}Ti	1.48E-07	1.19E-09	5.39E-09
^{21}Ne	2.74E-06	8.55E-05	4.15E-05	^{48}Ti	2.77E-05	2.15E-04	3.68E-04
^{22}Ne	1.43E-03	3.70E-02	2.45E-02	^{49}Ti	2.30E-06	1.79E-10	7.01E-09
^{23}Na	1.60E-04	1.18E-02	5.33E-03	^{50}Ti	1.02E-08	7.94E-20	3.67E-18
^{24}Mg	4.63E-04	2.97E-02	2.08E-02	^{50}Cr	1.01E-05	3.58E-08	1.49E-07
^{25}Mg	5.51E-04	1.13E-02	8.89E-03	^{52}Cr	4.31E-04	1.39E-03	2.66E-03
^{26}Mg	1.85E-03	1.52E-02	9.90E-03	^{53}Cr	1.03E-04	1.76E-08	6.34E-08
^{27}Al	1.35E-03	4.31E-03	2.56E-03	^{54}Cr	2.67E-08	5.77E-11	5.80E-12
^{28}Si	9.19E-03	1.42E-02	1.33E-02	^{55}Mn	1.56E-03	6.20E-08	3.70E-07
^{29}Si	8.32E-03	9.68E-02	1.05E-01	^{54}Fe	6.83E-04	3.19E-07	2.28E-06
^{30}Si	1.09E-05	7.40E-03	1.10E-02	^{56}Fe	4.40E-02	2.33E-01	2.84E-01
^{31}P	2.19E-03	2.97E-02	3.58E-02	^{57}Fe	7.78E-04	5.37E-05	8.75E-05
^{32}S	5.35E-03	3.97E-02	3.80E-02	^{59}Co	8.86E-06	2.90E-06	3.61E-06
^{33}S	1.72E-03	6.64E-02	9.82E-02	^{58}Ni	4.83E-04	4.40E-04	6.57E-04
^{34}S	4.31E-06	4.10E-03	7.46E-03	^{60}Ni	3.07E-04	2.17E-03	7.36E-03
^{35}Cl	4.13E-04	1.71E-02	3.40E-02	^{62}Ni	1.41E-06	9.50E-06	1.67E-04
^{37}CL	1.34E-04	1.90E-02	2.56E-02	^{63}Cu	1.78E-08	4.70E-07	2.61E-07
^{36}Ar	1.71E-03	2.39E-02	4.63E-02	^{65}Cu	3.99E-09	1.66E-08	1.02E-06
^{38}Ar	4.78E-06	2.28E-03	3.56E-03	^{64}Zn	2.17E-06	1.28E-05	8.75E-05
^{39}K	4.41E-05	8.04E-03	1.57E-02	^{66}Zn	3.31E-10	3.67E-09	8.05E-08
^{41}K	1.53E-05	1.36E-02	1.21E-02	^{56}Ni	4.39E-02	2.32E-01	2.84E-01
^{40}Ca	2.54E-03	5.08E-02	5.96E-02	^{56}Ni$_{\rm Jet}$	2.65E-02	2.30E-01	1.95E-01
^{44}Ca	1.05E-05	1.71E-03	2.06E-02	^{56}Ni$_{\rm SN}$	1.75E-02	2.29E-03	8.82E-02

Table 3: Abundance of heavy elements in the ejecta. Abundances are in units of $M_\odot$. All unstable nuclei produced in the ejecta are assumed to decay to the corresponding stable nuclei. The amount of ^{56}Ni is also in shown in the last row. We define the ^{56}Ni$_{\rm Jet}$ as the one within the 10° cone around the rotation axis at the final stage of the calculation, and the left we call as ^{56}Ni$_{\rm SN}$ in this study.